Self-adaptive transition of laser mode-locking states via online dispersion engineering over a wide range

ZIMIN ZHA[1], SUWAN SUN[1], KAILIN WU[1], ZHIMING SHI[1], YONGYUAN CHU[1], ZILONG LI[1,2], AND HAIRUN GUO[1,*]

[1] *Key Laboratory of Specialty Fiber Optics and Optical Access Networks, Joint International Research Laboratory of Specialty Fiber Optics and Advanced Communication, Shanghai Institute for Advanced Communication and Data Science, Shanghai University, Shanghai, China*
[2] *School of Engineering and Materials Science, Queen Mary University of London, Mile end, Bethnal Green, E1 4NS, London, United Kindom*
[*] *hairun.guo@shu.edu.cn*

Compiled August 25, 2023

We demonstrate dispersion engineered dissipative soliton mode locked lasers, by means of intracavity spatial light modulation (SLM). The inline cavity GVD control of wide range ($-0.28\,ps^2 \sim 0.06\,ps^2$) in the laser cavity is realized, by which we achieve continuous and stable switching of traditional solitons, dispersion-managed solitons and dissipative solitons. A transient process of pulse-adaptive reconstruction is observed during the switching of different solitons. Transitions of soliton dispersive waves from Kelly sidebands, and transforms to quartic solitons have been observed via tuning the high-order dispersion coefficients. w-shaped solitons are demonstrated under negitive second-order dispersion and positive fourth order dispersion.

http://dx.doi.org/10.1364/ao.XX.XXXXXX

Nonlinear systems with periodic variations of nonlinearity and dispersion occur in a variety of physical problems and engineering applications. Solitons are one of the most widely studied forms of excitation in nonlinear systems.[1] As local structures that can be seen as self-reinforcing waves, they propagate while maintaining the shape, which is a remarkable property that is achieved by balancing diffusion and focusing effects. In optics, solitons arise from the linear and nonlinear interaction of light and matter, and the soliton effect greatly improves the performance of the mode-locked laser and allows the direct generation of optical pulses with an ultra-short duration much less than 100fs.[2] Considerable engineering and technical efforts have been invested into the development of solid-state, fiber, and semiconductor lasers,[3] meanwhile, fiber lasers that can achieve mode-locking at a moderate energy scale are widely used in optical frequency comb[4–6], medical imaging, ophthalmology and so on[7–9].

During the propagation of solitons, the interaction between dispersion and nonlinear effects plays an outstanding role in shaping pulses and manipulating photodynamics. Stable pulse generation relies on careful laser design to achieve compensation between the various effects. As an implementation platform for soliton pulse, the fiber lasers do an excellent job in flexible design, with its unprecedented ability to engineer cavity dispersion through choice and length of fibre components, which leads to many new pulse behaviors and laser operation mechanisms, like dispersion-managed solitons and dissipative solitons[10–12].

Different dispersion environments bring not only pulse energy selectivity, but also the ability to generate, control and manipulate ultrashort light pulses and special waveforms. Therefore, the precise control of the cavity dispersion is required, exactly. In general cases, once the laser is built, the cavity become difficult to reconstruct with its fixed parameters. In order to achieve a higher degree of control of the pulse dynamics in the laser cavity, flexible dispersion tuning and editing of the cavity environment are very critical. The use of grating pairs[13] or a Martineztype stretcher[14, 15] with the insertion of an adjustable mechanical slit inside the cavity is a commonly employed method. However, these methods make the laser system complex and lack the precision as filters. And, due to mechanistic constraints, these schemes may provide a fixed, nontunable dispersion value that provides hysteretic dispersion change, and may be difficult to edit the dispersion in a wide range that continuously acrosses several dispersion regions. Recently, several online modes of regulating intra-cavity dispersion have been developed, which include spatial light modulation techniques[16]. That is, the modulation of the spectral amplitude and phase to obtain the designed optical waveform, has been widely used in many fields[17–20].

In this Letter, we have applied inline dispersion engineering in a NPR mode-locked fiber laser with spatial optical modulation. The continuous and stable switching from negative dispersion to positive dispersion is achieved, and it is observed that the switching between different soliton pulses working in different dispersion areas will undergo an adaptive reconstruction process which will arise a environmental stability related chaotic state in time domain. Besides, high-order dispersion engineering was achieved. By changing both third-order(TOD) and forth-order dispersion(FOD) components, we observed transitions of soliton dynamics, i.e. the emergence of soliton dispersive waves and the emergence of quartic solitons as well as the w-shaped solitons.

The experiment is based on a mode-locked fiber laser with nonlinear polarization rotation (NPR), cf. the schematic setup in Fig.1(a). The overall cavity length is 10.94 m with a 2.2 m

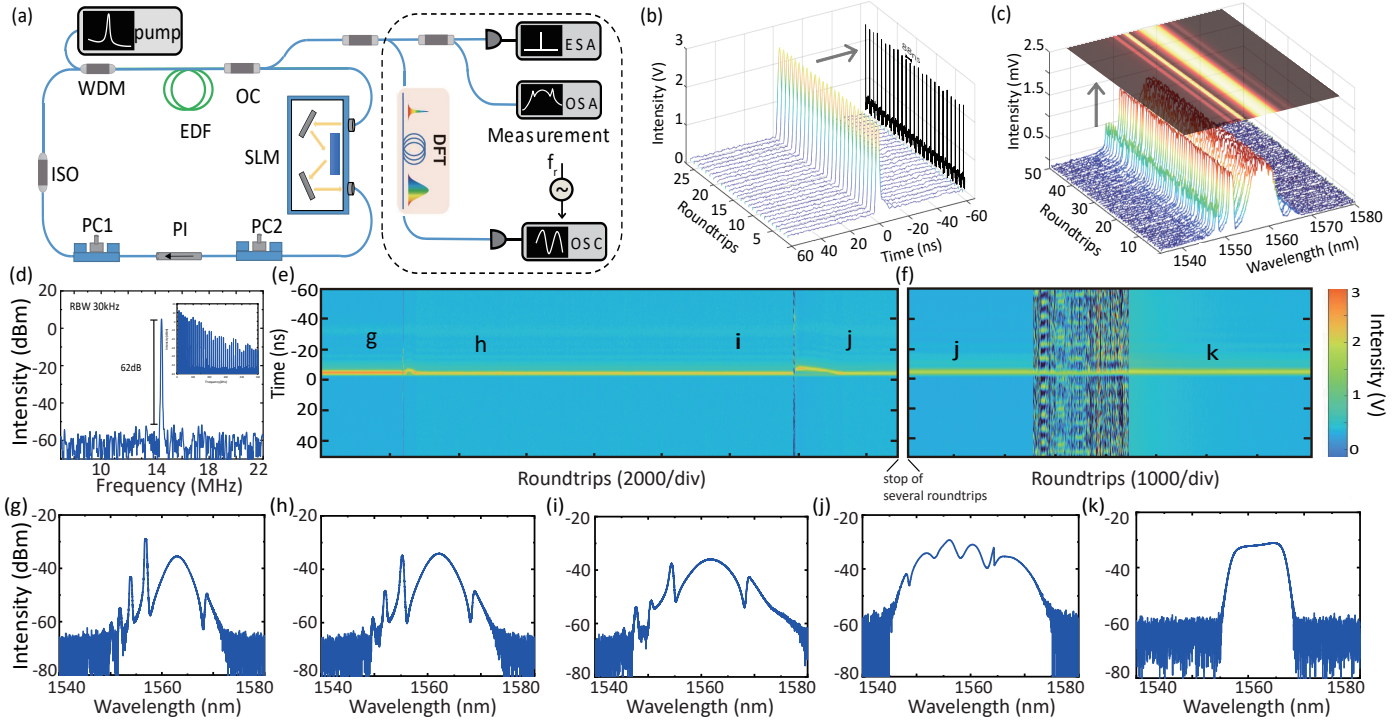

Fig. 1. Experimental (a) Setup of the NPR fiber laser. (b) Pulses in 3D view and pulse train on the yOz plane. (c) DFT spectrum in 3D view and top view. (d) Radio frequency spectrum. (e) Top view of the pulse train with continuous changed GVD from $-0.2739\,\mathrm{ps}^2$, $-0.2192\,\mathrm{ps}^2$, $-0.1645\,\mathrm{ps}^2$ to $-0.0551\,\mathrm{ps}^2$. (f) Top view of the pulse train for the switching between traditional soliton($-0.2739\,\mathrm{ps}^2$) and dispersion-managed soliton($-0.0551\,\mathrm{ps}^2$). (g-k) Optical spectra with the GVD at $-0.2739\,\mathrm{ps}^2$, $-0.2192\,\mathrm{ps}^2$, $-0.1645\,\mathrm{ps}^2$, $-0.0551\,\mathrm{ps}^2$ and $0.0543\,\mathrm{ps}^2$ respectively.

Erbium-doped fiber as gain fiber. the net cavity dispersion is ca. $-0.2375\,\mathrm{ps}^2$. Different from the ordinary NPR mode-locked fiber laser, a spatial light modulation module (Finisar WaveShaper4000A) is connected in the cavity, which is programmable in engineering cavity loss and phase spectral profile:

$$\phi(\omega) = L\sum_{n=2}^{4}\frac{\beta_n\omega^n}{n!} \tag{1}$$

Thus, we can set the phase mask within the bandwidth of the spectral pulse shaping at its frequency resolution of 10GHz so as to manipulate the cavity dispersion environment.

In the initial state (i.e. the SLM is fully transparent with no change on the phase), adjusting the angle of the polarization controller appropriately a soliton mode-locked laser is implemented by launching the pump power of 200 mW, which is characterized in both the temporal and spectral domain, cf. the results in Fig.1(b-d). An external Trigger signal whose frequency was consistent with the laser repetition frequency was used when measuring the DFT spectrum, to maintain the tracking of the signal. Due to the presence of spatial light modulators, there is additional dispersion, and the second-order dispersion at this time is estimated by the dispersion compensation to be about $-0.2739\,\mathrm{ps}^2$. In details, the laser spectrum is centered at the wavelength of ca. 1563.12 nm, with a 3-dB bandwidth of ca. 3.1 nm (Fig.1(g)), and a stable output pulse sequence with an interval of about 88 ns is obtained. The radio spectrum of the pulse sequence is also characterized (Fig.1(d)), where the fundamental frequency tone is 14.1 MHz, and the signal-to-noise ratio (SNR) is > 62 dB.

The value of the second-order dispersion in the cavity was adjusted by setting different phase masks. The pump power and polarization controller angle remain constant. When the cavity GVD was set at $-0.0551\,\mathrm{ps}^2$, the dispersion-managed soliton working in the near-zero dispersion region can be immediately obtained. A Gaussian spectrum which has a 3-dB bandwidth of ca. 21.44 nm (Fig.1(j)) was obtained while spectral sidebands were eliminated. Moreover, the dispersion-managed soliton can be obtained within a certain dispersion interval, about $-0.0824\,\mathrm{ps}^2 \sim -0.004\,\mathrm{ps}^2$, and slightly adjusting the angle of the polarization controller will not destroy the soliton state.

While the near-zero dispersion managed soliton was working, we could change the inner-cavity second-order dispersion to achieve dissipative solitons working in the net-normal dispersion region. Meanwhile, the bandwidth of the filter also requires proper control, as the DS requires additional amplitude modulation in addition to saturated absorber action. A Gaussian spectral profile is programmed on the filter because the default rectangular profile is similar to the shape of the DS spectrum. Fig.1(k) gives the DS spectrum obtained for the net GVD of $0.0543\,\mathrm{ps}^2$ and the filter's bandwidth at FWHM of 0.4 THz. The spectrum has the steep edges on its spectrum, and the bandwidth of it is limited at about 7.79 nm(3-dB bandwidth), these all were viewed as the features of DSs.

Due to the dispersion adjustment in the experiment was real-time and immediate, when the experimental parameters were set on the platform, continuous dispersion modification was carried out without changing any setting of the platform (such as pump power, polarization controller angle), so as to record the dynamic

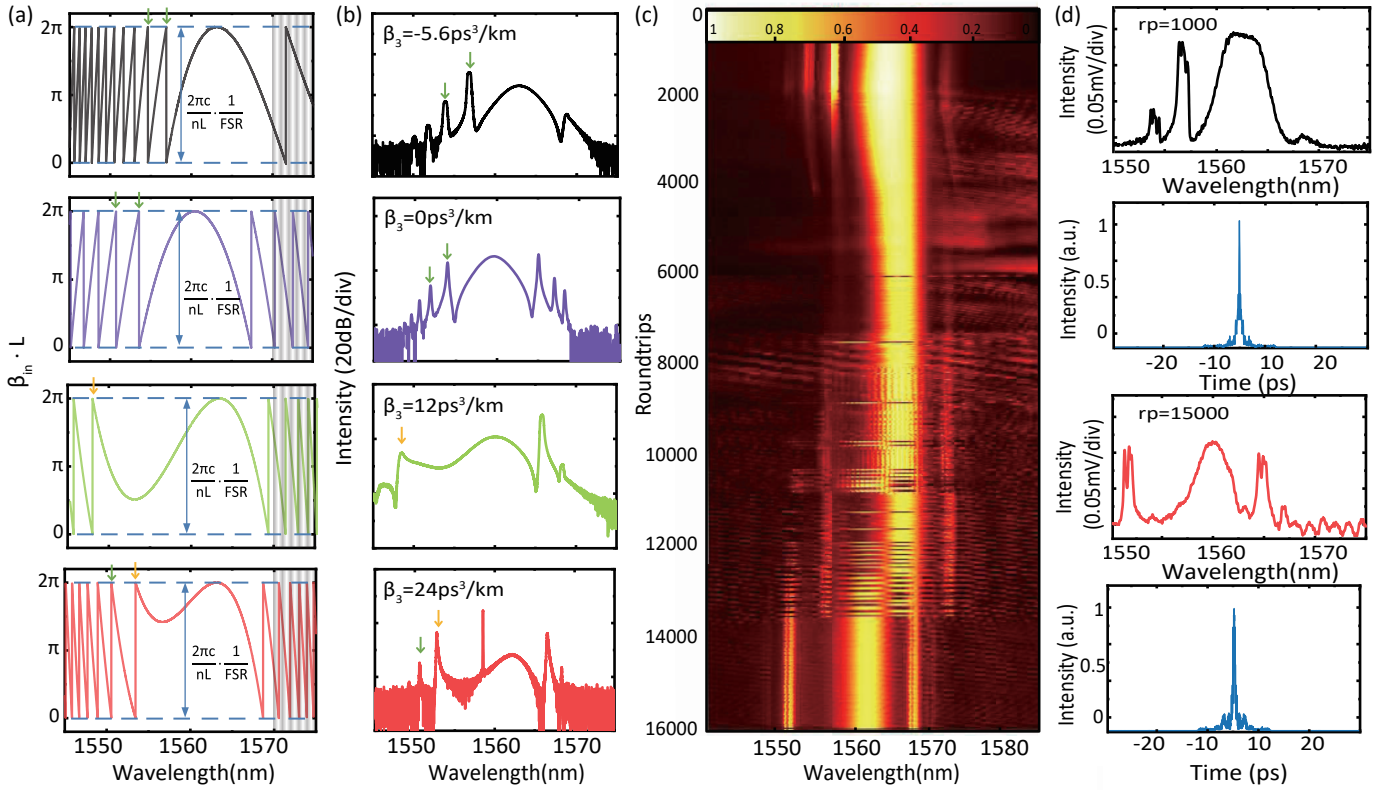

Fig. 2. Experimental (a) Cavity dispersion distribution curves with GVD at $-0.2739\,\mathrm{ps}^2$ and β_3 at $-5.6\,\mathrm{ps}^3/\mathrm{km}$, $0\,\mathrm{ps}^3/\mathrm{km}$, $12\,\mathrm{ps}^3/\mathrm{km}$ and $24\,\mathrm{ps}^3/\mathrm{km}$, respectively. The shadow parts are out of the bandwidth of SLM. The green arrows mark the position of the Kelly sidebands and the yellow arrows mark the dispersive waves. (b) Spectra corresponding to the curves in (a). (c) DFT spectrum when β_3 changed from $-5.6\,\mathrm{ps}^3/\mathrm{km}$ to $24\,\mathrm{ps}^3/\mathrm{km}$. (d) DFT spectrum and autocorrelation extracted from the process at 1000 roundtrip. (e) DFT spectrum and autocorrelation extracted from the process at 15000 roundtrip.

process of the soliton switching timely. Shown in Fig.1(e) at around 10000 roundtrip and in Fig.1(f), there was a chaotic state at the moment of switching, where the soliton pulse undergone an adaptive reconstruction process. The time length of the whole chaotic state was mainly related to the environmental stability of the laser and the process did not occur if the dispersion was slowly changed within a single region, shown in the 0 to 9900 roundtrips in Fig1(e), corresponding to the spectra in Fig.1(f-i).

Note that the soliton laser spectrum was not symmetric with respect to its center, as there could be intrinsic TOD or higher-order dispersion in the laser cavity. Therefore, we obtained a conventional soliton by compensating the higher-order dispersion presented in the cavity. With $5.6\,\mathrm{ps}^3/\mathrm{km}$ of added TOD, the soliton spectrum transformed into a symmetric structure. Increasing the cavity TOD, the first-order sideband closest to the center of the spectrum translated into a dispersive wave. And, as the TOD continued to increase, the sidebands became more compact and the dispersive wave got stronger with Kelly sidebands followed(Fig.2(b)). Similar features were seen from the shape of the dispersion curve, as shown in Fig.2(a). We then preformed a DFT analysis for the switching, shown in Fig.2(c), the evolution of the Kelly sideband and dispersive wave was obtained, and d shows the DFT spectra with certain characteristics extracted from the process at around 1000 and 15000 roundtrips(Fig.2(d)). It could be seen that with increasing TOD, the Kelly sideband translated into the dispersive wave. The spectrum first shrinks, then, the sidebands vanished followed by a competition of two spectral types. Finally, the dispersive wave became the dominant at around 1550 nm.

The whole evolution process experienced a certain length of time period, so we needed enough oscilloscope sampling time to achieve accurate sampling. Due to the limitation of oscilloscope bandwidth and sampling rate, the number of sampling rounds was too much to get enough range for DFT measurement. Thus, we sampled the spectra of each roundtrip separately by the history sampling pattern of the oscilloscope then integrated them in order before data processing. In this way, we can have sufficient spectral resolution and observe the spectral fine structures.

We draw a conclusion that due to the introduction of a strong TOD, the dispersion distribution curve shows the shape of the third-order function which has an inflection point in the presence of a distinct second-order dispersion. From center to the inflection point, the intensities of the corresponding frequency components show a corresponding rise. Because it does not reach to a FSR, the dispersion curve won' t fold but have a smooth bulge on the spectrum, in the form of a dispersion wave. We then increased the value of the TOD, and the variation in the dispersion distribution curve was also reflected in the shape of the output spectrum. That is, when the dispersion difference accumulated to a FSR, the intensity of the frequency component had a steep increasing state due to the curve's folding, and then the sharply shaped Kelly sidebands appeared. Within some allowable error limits, the positions of the fundamental dispersion wave and the Kelly sidebands corresponded to the positions of the inflection point and the folding point, respectively.

Obviously, the above process caused a asymmetrical change

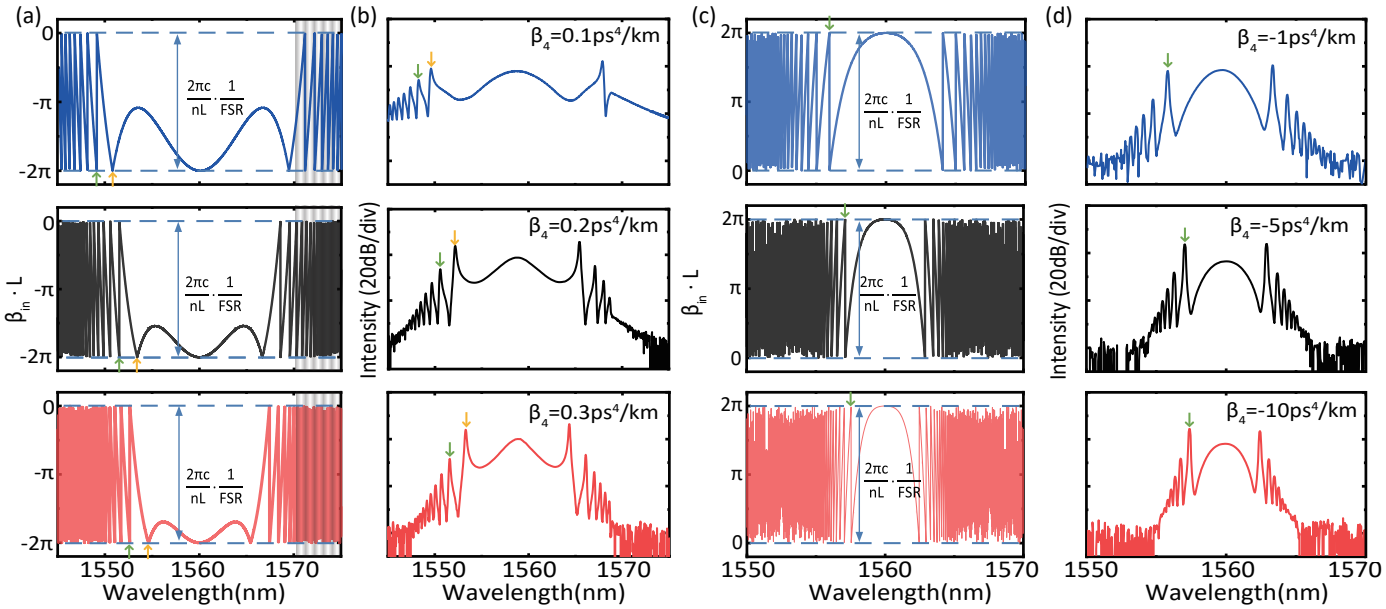

Fig. 3. Experimental (a) Cavity dispersion distribution curves with GVD at $-0.2739\,\mathrm{ps}^2$ and β_4 at $0.1\,\mathrm{ps}^4/\mathrm{km}$, $0.2\,\mathrm{ps}^4/\mathrm{km}$ and $0.3\,\mathrm{ps}^4/\mathrm{km}$, respectively. The shadow parts are out of the bandwidth of SLM. The green arrows mark the position of the Kelly sidebands and the yellow arrows mark the dispersive waves. (b) Spectra corresponding to the curves in (a). (c) Cavity dispersion distribution curves with GVD at $-0.2739\,\mathrm{ps}^2$ and β_4 at $-1\,\mathrm{ps}^4/\mathrm{km}$, $-5\,\mathrm{ps}^4/\mathrm{km}$ and $-10\,\mathrm{ps}^4/\mathrm{km}$. (d) Spectra corresponding to the curves in (c).

of the spectral sidebands because the dispersion distribution curve was a monotonic function and the inflection point occurred only on one side. In fact, this effect can be applied to both sides of the spectrum, which requires the introduction of higher and even order dispersion to allow inflection points to exist on both sides of the dispersion curve. Thus, along with the existence of a negative second order dispersion, we introduced a significant positive FOD to obtain a centrosymmetric dispersion distribution. Shown in Fig.3, as can be seen from the spectrum, the first-order sideband was the shape of the dispersion wave, corresponding to the 'w' shape of the dispersion distribution curve(Fig.3(a) and 3(b)). Other dispersion features were represented on the symmetrically distributed Kelly sidebands. When changing the sign of the FOD, the 'w' feature of the dispersion curve vanished, and the the spectrum's two sides translated into Kelly sidebands(Fig.3(c) and 3(d)). And, by, we could extract wavelength-dependent cavity dispersion in the gain band of the fiber cavity, which corroborates with the values introduced by the SLM.

In conclusion, we designed a NPR mode-locked fiber laser based on spatial optical modulation for dispersion engineering. The inline cavity GVD control of wide range ($-0.28\,\mathrm{ps}^2$~$0.06\,\mathrm{ps}^2$) in the laser cavity is realized, by which we achieved continuous and stable switching of traditional solitons, dispersion-management solitons and dissipative solitons. A transient process of pulse-adaptive reconstruction is observed for different types of soliton switching within the same laser, corresponding to the transient chaotic states in the time domain. Under the wide-range control of high-order dispersion (including TOD and FOD), we observed the emergence of dispersive waves and their evolution. Meanwhile, when there exists positive FOD in the anomalous GVD region, w-shaped solitons were obtained.Our work provides a convenient way to operate on a wide range of dispersion, giving new thinking for the study of soliton dynamics.

Funding. National Key Research and Development Program of China (2020YFA0309400); National Natural Science Foundation of China (11974234); Shanghai Science and Technology Development Foundation (20QA1403500).

Disclosures. The authors declare no conflicts of interest.

REFERENCES

1. R. Hirota, J. Math. Phys. **14**, 805 (1973).
2. D. E. Spence, P. N. Kean, and W. Sibbett, Opt. Lett. **16**, 42 (1991).
3. W. Sibbett, A. A. Lagatsky, and C. T. A. Brown, Opt. Express **20**, 6989 (2012).
4. S. T. Cundiff and J. Ye, Rev. Mod. Phys. **75**, 325 (2003).
5. T. Herr, V. Brasch, J. D. Jost, C. Y. Wang, N. M. Kondratiev, M. L. Gorodetsky, and T. J. Kippenberg, Nat. Photonics **8**, 145 (2014).
6. T. J. Kippenberg, A. L. Gaeta, M. Lipson, and M. L. Gorodetsky, Science **361**, eaan8083 (2018).
7. R. R. Gattass and E. Mazur, Nat. Photonics **2**, 219 (2008).
8. A. Prylepa, G. Luckeneder, K. H. Stellnberger, and D. Stifter, Laser Phys. **24**, 045407 (2014).
9. N. Nishizawa, Jpn. J. Appl. Phys. **53**, 090101 (2014).
10. E. Pincemin, O. Audouin, B. Dany, and S. Wabnitz, J. Light. Technol. **19**, 624 (2001).
11. D. Baccanari, A. Phillips, S. Smith, D. Sinski, and J. Burchall, Biochemistry **14**, 5267 (1975).
12. A. Chong, J. Buckley, W. Renninger, and F. Wise, Opt. Express **14**, 10095 (2006).
13. J.-H. Lin, C.-L. Chen, C.-W. Chan, W.-C. Chang, and Y.-H. Chen, Opt. Lett. **41**, 5310 (2016).
14. F. Haxsen, D. Wandt, U. Morgner, J. Neumann, and D. Kracht, Opt. Express **18**, 18981 (2010).
15. K. Underwood and J. T. Gopinath, Opt. Lett. **41**, 5393 (2016).
16. A. M. Weiner, Rev. Sci. Instruments **71**, 1929 (2000).

17. S. Boscolo, C. Finot, H. Karakuzu, and P. Petropoulos, Opt. Lett. **39**, 438 (2014).
18. M. Nakazawa, M. Yoshida, and T. Hirooka, Optica **1**, 15 (2014).
19. J. Peng and S. Boscolo, Sci. Reports **6**, 25995 (2016).
20. R. Iegorov, T. Teamir, G. Makey, and F. Ö. Ilday, Optica **3**, 1312 (2016).

FULL REFERENCES

1. R. Hirota, "Exact envelope-soliton solutions of a nonlinear wave equation," J. Math. Phys. **14**, 805–809 (1973).
2. D. E. Spence, P. N. Kean, and W. Sibbett, "60-fsec pulse generation from a self-mode-locked ti:sapphire laser," Opt. Lett. **16**, 42 (1991).
3. W. Sibbett, A. A. Lagatsky, and C. T. A. Brown, "The development and application of femtosecond laser systems," Opt. Express **20**, 6989 (2012).
4. S. T. Cundiff and J. Ye, "*Colloquium* : Femtosecond optical frequency combs," Rev. Mod. Phys. **75**, 325–342 (2003).
5. T. Herr, V. Brasch, J. D. Jost, C. Y. Wang, N. M. Kondratiev, M. L. Gorodetsky, and T. J. Kippenberg, "Temporal solitons in optical microresonators," Nat. Photonics **8**, 145–152 (2014).
6. T. J. Kippenberg, A. L. Gaeta, M. Lipson, and M. L. Gorodetsky, "Dissipative kerr solitons in optical microresonators," Science **361**, eaan8083 (2018).
7. R. R. Gattass and E. Mazur, "Femtosecond laser micromachining in transparent materials," Nat. Photonics **2**, 219–225 (2008).
8. A. Prylepa, G. Luckeneder, K. H. Stellnberger, and D. Stifter, "Low coherence interferometric second harmonic generation microscopy for non-destructive material testing using a broadband 1550 nm fs-fiber laser," Laser Phys. **24**, 045407 (2014).
9. N. Nishizawa, "Ultrashort pulse fiber lasers and their applications," Jpn. J. Appl. Phys. **53**, 090101 (2014).
10. E. Pincemin, O. Audouin, B. Dany, and S. Wabnitz, "Stability of synchronous intensity modulation control of 40-gb/s dispersion-managed soliton transmissions," J. Light. Technol. **19**, 624–635 (2001).
11. D. Baccanari, A. Phillips, S. Smith, D. Sinski, and J. Burchall, "Purification and properties of escherichia coli dihydrofolate reductase," Biochemistry **14**, 5267–5273 (1975).
12. A. Chong, J. Buckley, W. Renninger, and F. Wise, "All-normal-dispersion femtosecond fiber laser," Opt. Express **14**, 10095 (2006).
13. J.-H. Lin, C.-L. Chen, C.-W. Chan, W.-C. Chang, and Y.-H. Chen, "Investigation of noise-like pulses from a net normal yb-doped fiber laser based on a nonlinear polarization rotation mechanism," Opt. Lett. **41**, 5310 (2016).
14. F. Haxsen, D. Wandt, U. Morgner, J. Neumann, and D. Kracht, "Pulse characteristics of a passively mode-locked thulium fiber laser with positive and negative cavity dispersion," Opt. Express **18**, 18981 (2010).
15. K. Underwood and J. T. Gopinath, "Control of the state of a mode-locked fiber laser using an intracavity martinez compressor," Opt. Lett. **41**, 5393 (2016).
16. A. M. Weiner, "Femtosecond pulse shaping using spatial light modulators," Rev. Sci. Instruments **71**, 1929–1960 (2000).
17. S. Boscolo, C. Finot, H. Karakuzu, and P. Petropoulos, "Pulse shaping in mode-locked fiber lasers by in-cavity spectral filter," Opt. Lett. **39**, 438 (2014).
18. M. Nakazawa, M. Yoshida, and T. Hirooka, "The nyquist laser," Optica **1**, 15 (2014).
19. J. Peng and S. Boscolo, "Filter-based dispersion-managed versatile ultrafast fibre laser," Sci. Reports **6**, 25995 (2016).
20. R. Iegorov, T. Teamir, G. Makey, and F. Ö. Ilday, "Direct control of mode-locking states of a fiber laser," Optica **3**, 1312 (2016).